Sedimentary Geology 455 (2023) 106483

Contents lists available at ScienceDirect

Sedimentary Geology

journal homepage: www.elsevier.com/locate/sedgeo

Chad's cabinet of icy curiosities: Sharpening the interpretation of subglacial and ice marginal environments during the LPIA glaciation of the Ennedi Plateau

Ricarda Wohlschlägl [a,*], Christoph Kettler [b], Daniel Paul Le Heron [a], András Zboray [c]

[a] Department of Geology, University of Vienna, Vienna, Austria
[b] Department of Sedimentary Geology, Geosphere, Vienna, Austria
[c] Fliegel Jezerniczky Expeditions, Newbury, United Kingdom

ARTICLE INFO

Article history:
Received 27 March 2023
Received in revised form 31 July 2023
Accepted 7 August 2023
Available online 14 August 2023

Dr. Massimo Moretti

Keywords:
Late Palaeozoic Ice Age
Chad
Ennedi
Ice streams
Marine-terminating ice sheet
Grounding zone wedge
Soft-sediment striated surfaces

ABSTRACT

The Ennedi Plateau in Chad in north-central Africa exposes an outstanding example of a palaeo-ice stream glacial landsystem of late Palaeozoic age, with an assemblage of geomorphological structures of comparable preservation quality to those found in Quaternary deglaciated landscapes. Satellite images and various methods to combine acquired satellite data (e.g. band-ratio technique) have been used to interpret proglacial, ice-marginal and subglacial structures. The main goal of the study is to produce a detailed and more in-depth analysis of newly found structures that enhance our understanding of ice sheet behaviour in the Ennedi Plateau during the LPIA. We report the first known evidence of soft-sediment striated surfaces from outcrop, testifying to the existence of a soft-deformable bed. This deformable bed interpretation can probably be upscaled to explain the extensive swarms of mega-scale glacial lineations mapped previously across the plateau. Furthermore, we identify the first known fully preserved grounding zone wedge (GZW), replete with three-dimensional geometry, in the rock record. This unique structure exhibits a well pronounced slope and a convex topography. Its presence allows the position of the former coastline to be reconstructed as it is assumed that ice streams terminated into a former ocean basin. Building on the studies by Le Heron (2018) and Kettler et al. (this issue), our analyses permit unprecedented insights into the behaviour of a significant, mid-latitude, marine-terminating ice sheet during the LPIA.

1. Introduction

A rich sedimentary archive of the Late Palaeozoic Ice Age (LPIA; 360 to 254.5 Ma; Fielding et al., 2023) is recorded over large parts of Gondwana (e.g. Montañez and Poulsen, 2013; Le Heron et al., 2021; Limarino and López-Gamundí, 2021; Rosa and Isbell, 2021; Montañez, 2022). In northern Africa the record is far less well known. Field description and subsequent interpretation of glacial deposits are restricted to Niger (Lang et al., 1991) and putative tillite layers in Egypt and Sudan (Klitzsch, 1983). The relatively recent discovery of a large, ancient glaciated landscape from satellite imagery in the Ennedi region in Chad considerably expands the known range of LPIA ice sheets on Gondwana (Le Heron, 2018). In terms of palaeo-glaciation, Ennedi is a blank canvas waiting to be painted by a wealth of new discoveries. This paper presents (i) the first geomorphological interpretation of a grounding zone wedge (GZW) in the pre-Cenozoic record which is indicative of a marine-terminating ice sheet (Batchelor and Dowdeswell, 2015; Demet et al., 2018), (ii) evidence of soft-sediment striated surfaces from outcrop, and (iii) the discovery of a newly found ice-stream pathway. In so doing, we shed new light on the palaeogeographic setting of the ice mass, with a focus on subglacial and ice-marginal conditions. We also showcase the value of the band-ratio technique and principal component analysis (PCA) of satellite image data to understand the geometry, crosscutting relationships, and preservation status of multiple generations of inverted channel systems interpreted to have developed in a proglacial setting during retreat phases. The Ennedi Plateau thus shows glacial landforms originating from an LPIA ice sheet as an exceptionally well-preserved analogue to Quaternary deglaciated areas, whilst providing insight into the glacial evolution in northern Africa, which has been significantly under investigated.

2. Geological setting and previous work

Chad is situated in north-central Africa. The northern area is characterised by the Sahara desert landscape whilst the more fertile zone in the south is part of the Sudanian Savanna (Brugière and Scholte, 2013).

* Corresponding author.
E-mail address: ricarda.wohlschlaegl@univie.ac.at (R. Wohlschlägl).

https://doi.org/10.1016/j.sedgeo.2023.106483

The study area (Ennedi Plateau; Fig. 1A) lies on the southernmost spur of the Erdis Basin, which is an extension of the Kufra Basin (Schlüter, 2006; Fig. 1B). The intracratonic basin forms a crustal depression filled with a succession of Palaeozoic and Mesozoic strata of shallow marine and fluvial origin (Lüning et al., 1999; Le Heron et al., 2014). Low-relief massifs, where most of the Proterozoic and Palaeozoic strata occur, are located on the flanks of the Kufra Basin and slope gently towards its centre (Gindre et al., 2012; Fig. 1B). During the LPIA, Ennedi and the Kufra Basin were located in the northern part of Gondwana within the South Polar Circle (Torsvik and Cocks, 2011, 2013; Lawver et al., 2014; Fig. 1C).

Marking the southern flank of the Erdis Basin, the Ennedi Plateau represents a vast sandstone complex (>50,000 km^2). To date, geological investigations have focussed on mapping and establishing a working stratigraphy, motivated by the need to find viable aquifers (Vogt et al., 2013). The geological framework of the Ennedi can be summarised as a gently dipping series of strata from Cambrian to Carboniferous age. Most of the exposed surface of the Ennedi Plateau is composed of Ordovician to Devonian strata and marine Carboniferous in the Mourdi Depression (Fig. 1D), with outcrops of Cambrian to Silurian age restricted to the south and southwest (Mahamoud, 1986; Klitzsch et al., 1993; Schlüter, 2006; Ghienne et al., 2023). In practice, the gentle northward dip of the plateau means formations and their constituent bedding surfaces can be traced for up to 500 km along strike (Wolff, 1964), lending the area the ideal characteristics for deep-time palaeo-geomorphological investigation (Le Heron et al., 2022). In terms of published work, however, stratigraphic investigations of the Ennedi lag considerably behind those undertaken at other flanks of the Kufra Basin (e.g. detailed Silurian-Devonian sequence stratigraphy at Jebel az-Zalmah in Libya; Gindre et al., 2012). Due to the scarcity of publications on the Ennedi Plateau, glacial palaeo-geomorphological investigations (the present paper plus the sister paper by Kettler et al., this issue) have been undertaken before fieldwork that could be used to provide detailed age constraints, as has been recently achieved in the LPIA basins of southern Africa (Griffis et al., 2021). However, given the available geological maps (Wolff, 1964; Mahamoud, 1986) the glacial phenomena discussed herein are constrained to the LPIA, considered to span an interval 360 to 254.5 Ma (i.e. Devonian to Permian) with no further

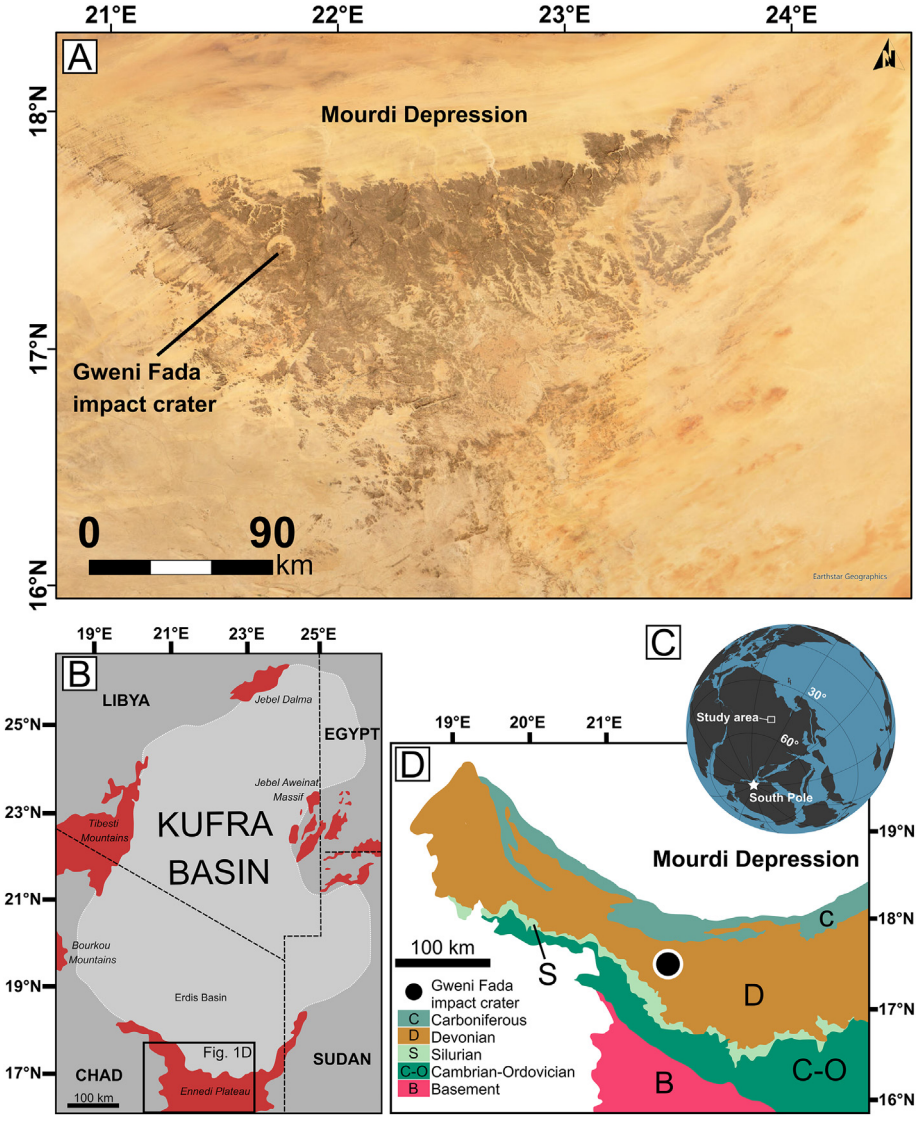

Fig. 1. (A) The Ennedi Plateau is a sandstone plateau situated amidst the Sahara Desert. To the north lies the Mourdi Depression filled with fluvial and marine sediments (Mahamoud, 1986; Klitzsch et al., 1993). (B) The Kufra Basin covers SE Libya, northern Chad, NW Sudan and parts of western Egypt (Le Heron et al., 2014). It is one of the largest intracratonic basins. The Erdis Basin is the Chadian part of the Kufra Basin. Its southernmost boundary is the Ennedi Plateau. (C) Location of the Ennedi Plateau on Gondwana during the early Carboniferous (~340 Ma; Gondwana reconstruction from Domeier and Torsvik, 2014, software: GPlates); (D) Simplified geological map of the Ennedi Plateau (modified after Wolff, 1964 and Le Heron et al., 2014). The palaeo-ice stream pathways are developed on a Devonian surface.

constraints available (Fielding et al., 2023). Marine carbonates from the Carboniferous in the Mourdi Depression (Mahamoud, 1986; Klitzsch et al., 1993) confirm the existence of a shoreline immediately north of the Ennedi by Tournaisian times at ~350 Ma (Torsvik and Cocks, 2013). The Ennedi Plateau itself is dominated by sandstones with cross-stratified units recording an interaction of fluvial and marine processes over time (Klitzsch et al., 1993; Vogt et al., 2013; Haeberlin et al., 2016). The westernmost part of the plateau (Ghienne et al., 2023) and the Sudanese part of the Ennedi in the far east have been described more comprehensively. Sedimentary logs from the Sudanese part show cyclic series of shallow marine claystones, siltstones and sandstones, which become coarser towards the top and are interspersed with thick fluviatile intercalations of sandstone sequences for the Devonian interval. The Carboniferous is preserved starting from the southern margin of the Mourdi Depression and does not appear on the plateau (Klitzsch et al., 1993).

2.1. Glacial evidence

During the Late Palaeozoic Ice Age (LPIA), the longest lasting and most severe glaciation of the Phanerozoic (Montañez and Poulsen, 2013), glaciers spread over large soft beds thus producing an abundance of soft sediment structures, such as striated surfaces (Le Heron et al., 2020). Glaciation began in Argentina during the Viséan. Ice centres then expanded over western and southern America and Australia. The maximum extent was reached during the Late Pennsylvanian (Isbell et al., 2012). Northern Africa was mostly located in the lower mid-latitudes during the LPIA (Lawver et al., 2014) and ice centres have thus far only been reported from Niger (Lang et al., 1991), with putative tillite layers from Sudan and Egypt (Klitzsch, 1983). The Ennedi Plateau thus adds to the LPIA record of glaciation in the northern parts of Gondwana and opens up discussions about possible glaciation in an area not tied to highlands.

Initial work on the palaeo-glacial structures in Ennedi was completed by Le Heron (2018), which was developed by Kettler et al. (this issue) with more extensive mapping. N-S trending palaeo-ice stream pathways, indicating a south to north palaeo-flow, were described along with associated features such as large-scale lineations, remnants of moraines represented by ridges at the margins of the palaeo-ice streams (Le Heron, 2018), and a possible meltwater channel system (Kettler et al., this issue). Palaeo-ice streams are areas of fast-flowing ice within an ice sheet and can be identified in the ancient record mostly by the occurrence of glacial troughs and large-scale glacial lineations (Stokes and Clark, 2001; Canals and Amblas, 2016). In addition to the expansion of the glacially influenced area a newly discovered system of inverted channels was also described (hereinafter referred to as Inverted Channel Assemblage, ICA; Fig. 2A, see also Figs. 3 and 4 in Kettler et al., this issue).

The numbering of ice streams from I to X, together with the term 'inverted channel assemblage' and the numbering of inverted channels (1–21, see Section 4.4) was specifically established in this paper and has not been previously used in Le Heron (2018) and Kettler et al. (this issue) (Fig. 2).

3. Methodology

3.1. Acquisition of satellite image data

ASTER, Landsat-8 and Sentinel-2 image data (Table 1) and digitised geological maps were used to enhance lithological differences, create

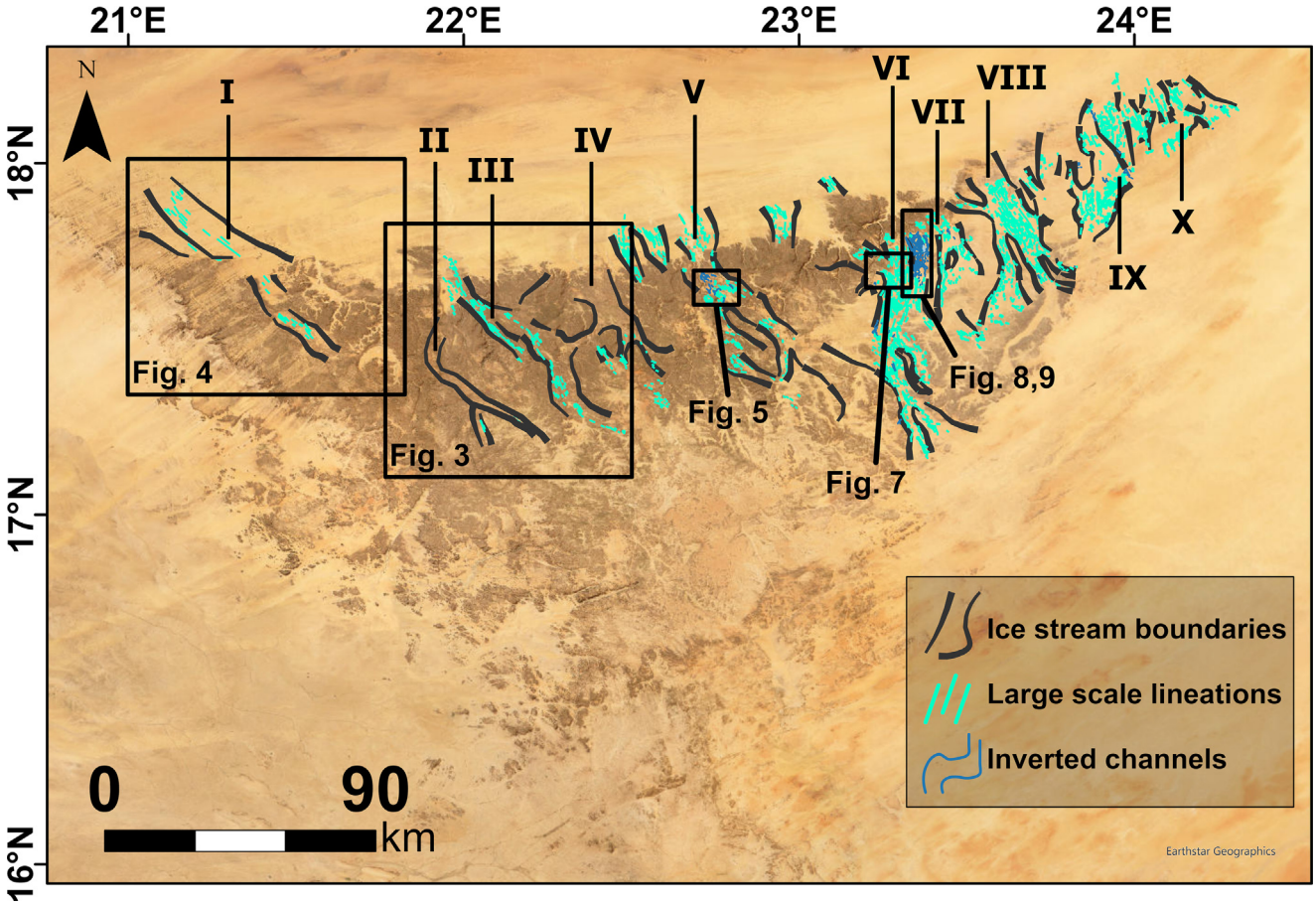

Fig. 2. Palaeo-ice stream pathways are represented by large-scale lineations and sharp boundaries. The structures are located on a Devonian surface with marine Carboniferous sediments to the north in the Mourdi Depression.

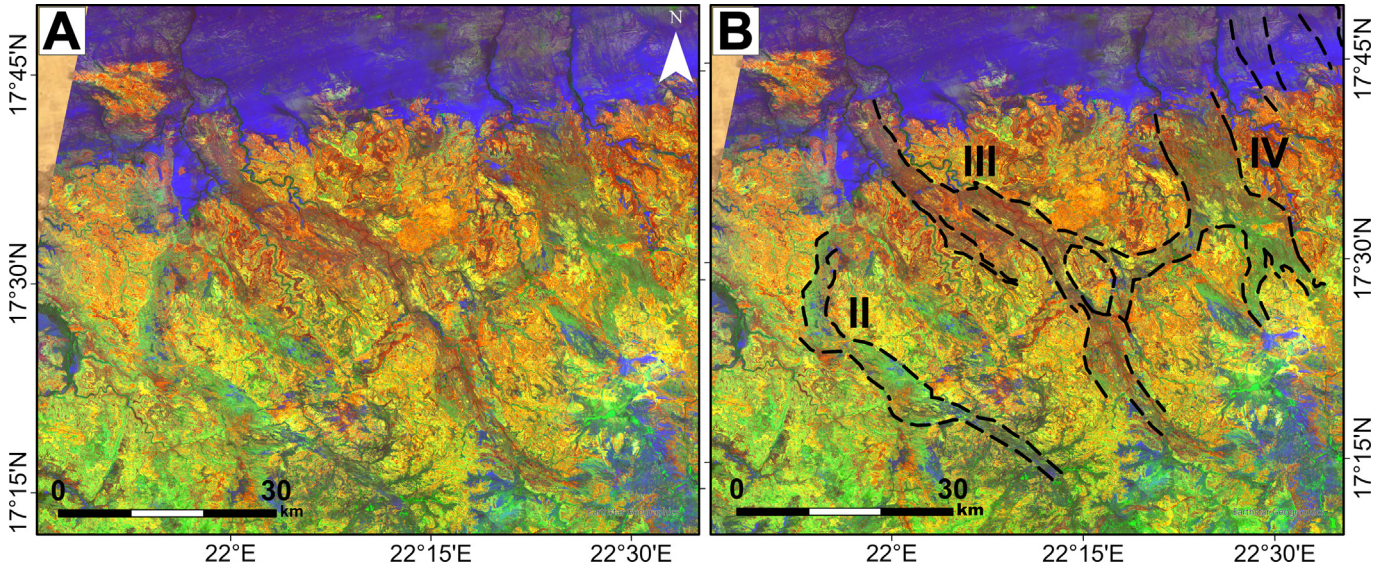

Fig. 3. (A) The Landsat-8 FCC of the west-central area of the Ennedi Plateau highlights differences in surface mineral composition (R: 6/5; G: 6/7; B: 4/2). Palaeo-ice stream pathways can be clearly differentiated from surrounding interstream areas with the band-ratio technique. The round structure to the left is the Gweni Fada crater. (B) Landsat-8 FCC from (A) with palaeo-ice stream boundaries (central coordinates: 17°29′17.1″N 22°01′32.0″E).

mineral maps and extract information not visible to the human eye. SRTM data (Shuttle Radar Topography Mission; spatial resolution: 30 m/pixel) enables the creation of Digital Elevation Models (DEMs), 3D models and height profiles. Identifying differences in lithology and surface mineral composition is possible due to various processing techniques (Section 3.2). Satellites carry different instruments which measure energy in different ranges of frequencies along the electromagnetic (EM) spectrum. These portions of frequencies are called bands. Combinations of bands can highlight specific minerals and mineral groups in so-called False Colour Composite images (FCCs; Richards and Jia, 2006). ASTER and Landsat-8, as well as SRTM images, were acquired via the Earth Explorer website of the United States Geological Survey (Earth Explorer, USGS, n.d). Sentinel-2 images were downloaded via the Copernicus Open Access Hub and the Sentinel Hub EO Browser. For Chad, resolutions up to 10 m per pixel (Sentinel images) are freely available, but most images have a lower spatial resolution between 30 m and 90 m per pixel (ASTER and Landsat images). ASTER Level 1T V3, Landsat-8 Collection 2 Level 2, and Sentinel-2 L1C and L2A were chosen because they are freely available and facilitate an overview of surface mineral composition.

In the course of a tourist expedition in 2016 (and revisited in 2021), A. Zboray visited an outcrop within one of the proposed palaeo-ice streams of Le Heron (2018) to investigate outcrop geomorphological evidence for glaciation. Apart from this, no field work has been possible.

3.2. Processing of satellite image data

Every mineral has a unique chemical composition and therefore its own spectral signature. The more spectral bands that cover a specific range of the EM spectrum, the more information can be extracted. Topographic slope, shadows and seasonal changes in sunlight angle and intensity can cause different brightness values of identical materials on the surface. Band rationing reduces these effects and creates images with unique colours for different ions/molecules. Satellite image pre-processing/processing was done in QGIS and ArcGIS. The QGIS 3.24. Plugin 'Raster Calculator' was used to divide bands by one another. This improves the contrast, enhances the spectral signatures and cancels out uneven illumination caused by topography (Osinowo et al., 2021). Band ratios may contain some false results due to the spectral interference of minerals with similar absorption and/or reflection properties. When using only band ratios for the preparation of a geological map of a study region, some of the spectral interference can result in lithological boundary discrimination with low accuracy and acquired data needs to be handled with care (Askari et al., 2018). To compensate for this, the PCA method (Principal Component Analysis) was also applied (Liu and Mason, 2016). Sentinel-2 Level 2 and Landsat-8 Level 2 data is already processed in terms of atmospheric, geometric and radiometric correction prior to download so no additional pre-processing techniques were applied (Suhet, 2015; Sayler, 2022). This study uses satellite images mainly to distinguish between different structures and enhances them with general surface mineral maps (Fig. 3). Therefore, no detailed surface mineral study is currently available and enhanced processing methods for satellite images have been avoided.

4. Results

Large-scale lineations and sharp boundaries mark trough-like areas distributed over the Ennedi Plateau from west to east that have been interpreted as ice stream pathways (Le Heron, 2018; Kettler et al., this issue).

In this study, we offer a detailed description of a newly discovered ice stream pathway in the extreme western part of the plateau (Section 4.1) as well as an introduction to newly found glacial structures such as striated surfaces (Section 4.2) and a grounding zone wedge (Section 4.3). Section 4.4 offers a more detailed approach at categorising the channel sediments of the suite of exhumed ridges (Inverted channel assemblage, ICA) first mentioned in Kettler et al. (this issue) based on selected criteria.

4.1. New palaeo-ice stream in the westernmost Ennedi

In addition to the established palaeo-ice stream network over the plateau (Kettler et al., this issue), new evidence for large-scale lineations and sharp lateral boundaries is presented herein, forming part of a newly discovered ice stream pathway starting at the western flank of the Gweni Fada crater and extending into the Mourdi Depression (Ice Stream I; Fig. 4). In this context, large-scale lineations are defined as elongate structures measuring up to several kilometres long (Stokes and Clark, 2002). The mostly parallel lineations occur in an area of approximately 1000 km^2, are partly sand-covered and less pronounced

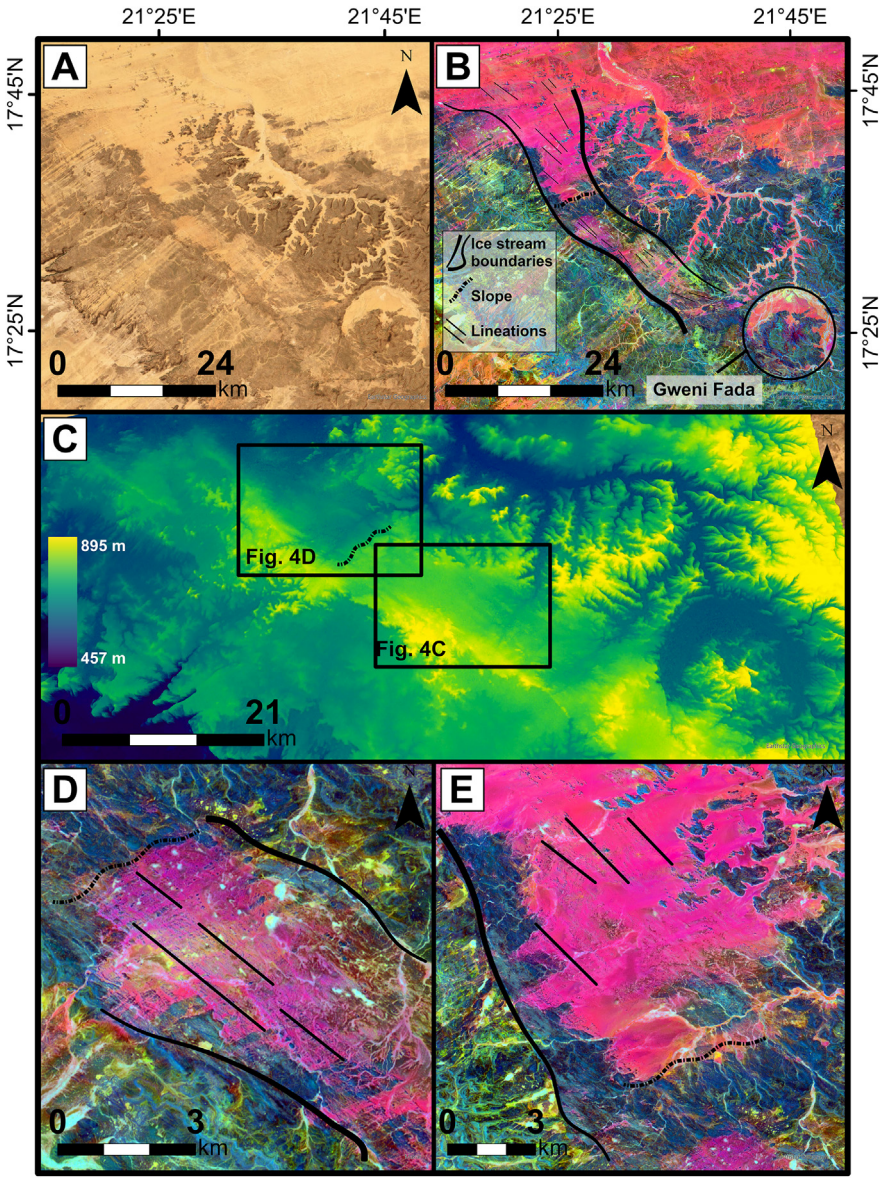

Fig. 4. (A) Location of Ice Stream I to the NW of the Gweni Fada crater. (B) Glacial features of Ice Stream I on a Sentinel 2 PCA image. (C) DEM; location of the sediment accumulation (slope) that separates two topographic layers of glacial lineations. Differences in elevation are noticeable. (D) Close-up of large-scale lineations at the upper part of the slope. (E) Close-up of large-scale lineations at the lower-lying part of the slope (central coordinates: 17°35′30.5″N 21°26′54.2″E).

than on Ice Streams III and VI, for example. About 31 km from the crater rim to the northwest is a slope where the large-scale lineations end abruptly. However, they continue northwest of this slope at an elevation around 100 m lower than those at the top (Fig. 4C). The slope (~9 %) has a length of about 4 km and a width of ~7 km. The nearby Gweni Fada crater is devoid of large-scale lineations.

The addition of an ice stream in the westernmost part of the Ennedi Plateau increases the proposed size of the Ennedi ice sheet. We interpret the location of the large-scale lineations on two discrete stratigraphic levels to the NW and SE of the slope area as evidence for sediment deposition between different phases of ice recession/advance.

4.2. Ground control: discovery of soft-sediment striated surfaces

Soft-sediment structures, such as striated surfaces, have the potential to record the temporal evolution of the subglacial environment, e.g. from fully grounded conditions to a floating margin (Le Heron et al., 2019). Impressive examples can be found in Africa (South Africa; Le Heron et al., 2019) and South America (Brasil; Vesely and Assine, 2014), amongst others.

The first record of soft-sediment striated surfaces in the LPIA in Chad is presented for Ice Stream V (Fig. 5). The ridges and grooves are usually parallel to one another and oriented approximately NNW-SSE (~340°N; Fig. 5C), and thus parallel to the large-scale lineations observed on satellite imagery. The distances between the grooves and ridges are a few centimetres. A thin dark patina covers the surface. The ridges and grooves have developed in fine-grained and argillaceous Devonian sandstone (Klitzsch et al., 1993; Vogt et al., 2013; Haeberlin et al., 2016).

The narrow and linear grooves and ridges are typical in the palaeorecord for ice moving over a soft-sediment surface, with identical geometries reported from the Late Ordovician record of northern Africa and Arabia (Senalp and Al-Laboun, 2000; Deynoux and Ghienne, 2004; Le Heron et al., 2005, 2010, 2020; Tofaif et al., 2018), or equally from the LPIA record of Ethiopia (Bussert, 2010), Brazil (Rocha-Campos et al., 2008; Rosa et al., 2016), Niger (Lang et al., 1991), or South Africa (Le

Table 1
Satellite image data.

Satellite	Dataset	Website	Product ID data sets	Spatial resolution (spectral bands)
Landsat-8	Collection 2, Level-2	Earth Explorer	LC08_L2SP_180048_20211008_20211018_02_T1	30 m (bands: 2, 3, 4, 5, 6, 7) 100 m (bands: 10, 11)
			LC08_L2SP_180048_20210720_20210729_02_T1	30 m (bands: 2, 3, 4, 5, 6, 7) 100 m (bands: 10, 11)
			LC08_L2SP_179048_20211204_20211209_02_T1	30 m (bands: 2, 3, 4, 5, 6, 7) 100 m (bands: 10, 11)
			LC09_L2SP_181048_20220503_20220505_02_T1	30 m (bands: 2, 3, 4, 5, 6, 7) 100 m (bands: 10, 11)
Sentinel-2	L1C, L2A	Sentinel Hub	2021-10-06-00_00_2021_10-06-23_59_Sentinel-2_L2A	10 m (bands: 2, 3, 4, 8) 20 m (bands 5, 6, 7, 8a, 11, 12)
			2021-10-06-00_00_2021_10-06-23_59_Sentinel-2_L1C	10 m (bands: 2, 3, 4, 8) 20 m (bands 5, 6, 7, 8a, 11, 12)
			2021-12-05-00_00_2021_12-05-23_59_Sentinel-2_L2A	10 m (bands: 2, 3, 4, 8) 20 m (bands 5, 6, 7, 8a, 11, 12)
			2021-12-05-00_00_2021_12-05-23_59_Sentinel-2_L1C	10 m (bands: 2, 3, 4, 8) 20 m (bands 5, 6, 7, 8a, 11, 12)
		Copernicus Hub	T34QHF_20210529T084601	10 m (bands: 2, 3, 4, 8) 20 m (bands 5, 6, 7, 8a, 11, 12)
			T34QHE_20210529T084601	10 m (bands: 2, 3, 4, 8) 20 m (bands 5, 6, 7, 8a, 11, 12)
			T34QEE_20210527T085559	10 m (bands: 2, 3, 4, 8) 20 m (bands 5, 6, 7, 8a, 11, 12)
			T34QFE_20210524T084559	10 m (bands: 2, 3, 4, 8) 20 m (bands 5, 6, 7, 8a, 11, 12)
			T34QFE_20210805T085559	10 m (bands: 2, 3, 4, 8) 20 m (bands 5, 6, 7, 8a, 11, 12)
			T34QGE_20210524T084559	10 m (bands: 2, 3, 4, 8) 20 m (bands 5, 6, 7, 8a, 11, 12)
			T34QDE_20211113T090129	10 m (bands: 2, 3, 4, 8) 20 m (bands 5, 6, 7, 8a, 11, 12)
SRTM	/	Earth Explorer	SRTM1N15E020V3 to SRTM1N15E023V3	30 m
			SRTM1N16E020V3 to SRTM1N16E023V3	30 m
			SRTM1N17E020V3 to SRTM1N17E023V3	30 m
			SRTM1N18E020V3 to SRTM1N18E023V3	30 m
			SRTM1N18E020V3 to SRTM1N18E023V3	30 m
ASTER	L1T	Earth Explorer	AST_L1T_00303092007090341_20150518142938_10903	15 m (bands: 1, 2, 3) 30 m (bands: 4, 5, 6, 7, 8, 9) 90 m (bands: 10, 11, 12, 13, 14)
			AST_L1T_00301012021090904_20210102075712_4332	15 m (bands: 1, 2, 3) 30 m (bands: 4, 5, 6, 7, 8, 9) 90 m (bands: 10, 11, 12, 13, 14)
			AST_L1T_00305102021204328_20210511122106_3097_T	15 m (bands: 1, 2, 3) 30 m (bands: 4, 5, 6, 7, 8, 9) 90 m (bands: 10, 11, 12, 13, 14)
			AST_L1T_00305102021204947_20210502122217_19937_T	15 m (bands: 1, 2, 3) 30 m (bands: 4, 5, 6, 7, 8, 9) 90 m (bands: 10, 11, 12, 13, 14)
			AST_L1T_00305102021204938_20210502093708_20144_T	15 m (bands: 1, 2, 3) 30 m (bands: 4, 5, 6, 7, 8, 9) 90 m (bands: 10, 11, 12, 13, 14)
			AST_L1T_00305082021205543_20210509114959_10500_T	15 m (bands: 1, 2, 3) 30 m (bands: 4, 5, 6, 7, 8, 9) 90 m (bands: 10, 11, 12, 13, 14)
			AST_L1T_00309182005090837_20150511053227_68470	15 m (bands: 1, 2, 3) 30 m (bands: 4, 5, 6, 7, 8, 9) 90 m (bands: 10, 11, 12, 13, 14)

Satellite image data sets used in this work. ASTER L1T data includes all bands and thermal bands. Sentinel-2 imagery was downloaded in both L1C (Top of Atmosphere) and L2A (Bottom of Atmosphere) quality. SRTM data includes 20 tiles covering the whole Ennedi Plateau with each row consisting of 4 tiles. All tiles have a cloud coverage of 0 %.

Heron et al., 2019; Fig. 6). Different origins are proposed (Bussert, 2010), e.g. (i) excavation by basal clasts (Goldthwait, 1979), (ii) subglacial deformation of till (Le Heron et al., 2005), (iii) subglacial meltwater erosion (Munro-Stasiuk et al., 2005), or (iv) iceberg keel marks (Woodworth-Lynas and Dowdeswell, 1994; Vesely and Assine, 2014; Isbell et al., 2023). Very similar structures can also be formed as shear zones in subaqueous slides, or due to ice-marginal glacio-tectonism (Jakobsson et al., 2008).

In the case of the Ennedi structures, the parallel orientation of soft-sediment striations to lineations mapped on satellite imagery, and thus parallel to regional ice flow, provides a strong contextual argument that these examples originate through subglacial shearing beneath an ice stream in soft sediment. Nevertheless, an alternative mechanism of iceberg keel grounding (Jakobsson and Anderson, 2016) cannot be ruled out without detailed fieldwork.

4.3. First geomorphological evidence for an LPIA grounding zone wedge (GZW)

At the northern reaches of Ice Stream VI, elevation profiles from SRTM data show a gentle southward-dipping slope with abundant glacial lineations which stop abruptly at a northward-dipping slope (~11 %) beyond which the glacial lineations are absent. SRTM digital elevation models show a relative elevation with respect to the wadi floor between 40 and 70 m. We therefore recognise a structure that has a convex shape and is positioned orthogonal to the large-scale glacial

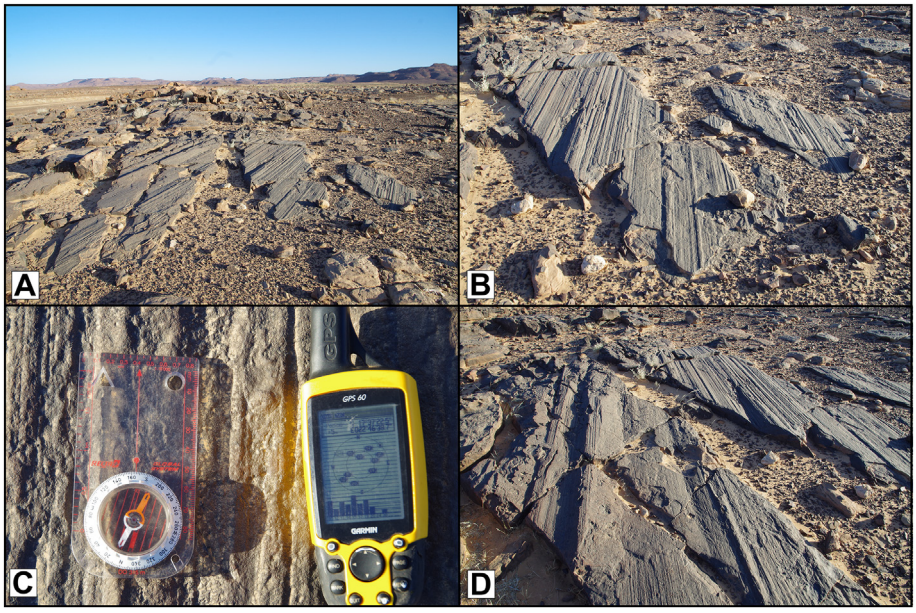

Fig. 5. (A–D) Striated surfaces on Ice Stream V. Parallel lineations were created by ice moving over soft sediment. Desert varnish forms a thin layer that highlights the structures. (Images from the field by A. Zboray; coordinates: 17°37′22.5″N 022°46′38.7″E).

lineations. The approximate width of this structure is 4 km and it is laterally constrained to the east by Ice Stream VII and to the west by an area with no visible glacial geomorphological features.

We interpret this structure as a GZW deposit (Fig. 7). GZWs form through sediment delivery by fast-flowing ice streams which explains the occurrence of the Ennedi GZW on the pathway of Ice Stream VI. The GZW shape is influenced by sediment input to the grounding zone, the width of the palaeo-ice stream, and the dimensions of the cavity between the ice and the grounding zone (Dowdeswell and Fugelli, 2012). GZWs are commonly observed on modern, high-latitude continental shelves within cross-shelf troughs and fjord systems where seaward-flowing ice decouples from its bed and starts to float

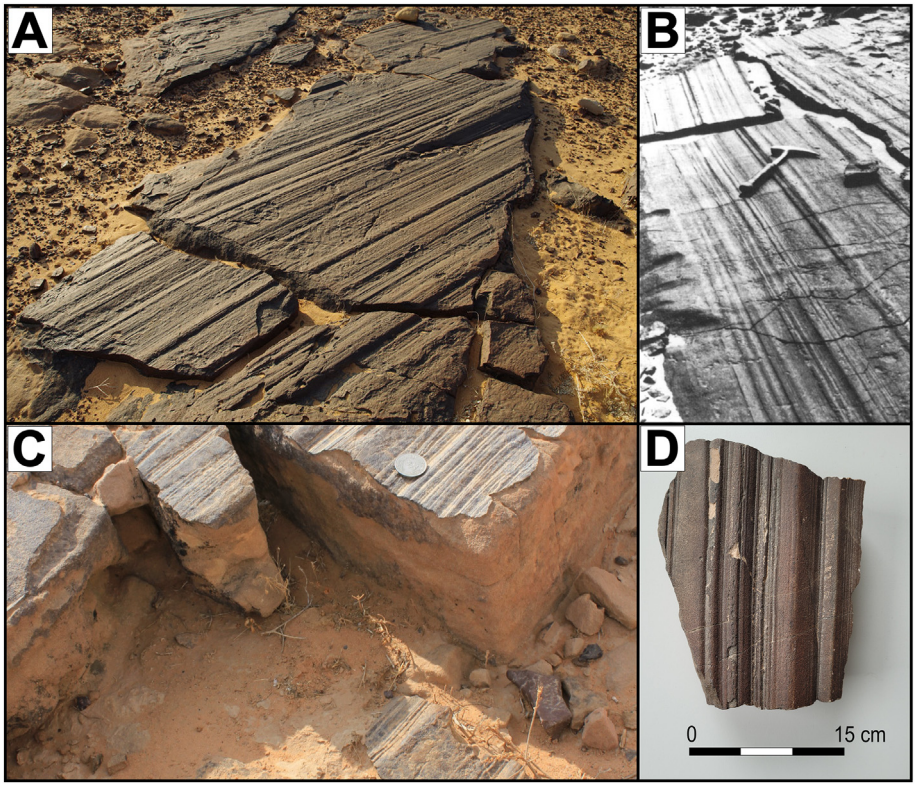

Fig. 6. Comparison of striated surfaces from the Palaeozoic in Africa. (A) Striated surfaces on Ice Stream V (Ennedi; coordinates: 17°37′22.5″N 022°46′38.7″E; image from A. Zboray); (B) soft-sediment striated surface (Ordovician) from Algeria interpreted as iceberg keel marks (Woodworth-Lynas and Dowdeswell, 1994). (C) Stacked subglacial soft sediment surfaces from Libya (Le Heron et al., 2020). (D) Soft sediment striated surface sample from Algeria (Late Ordovician; Le Heron et al., 2020).

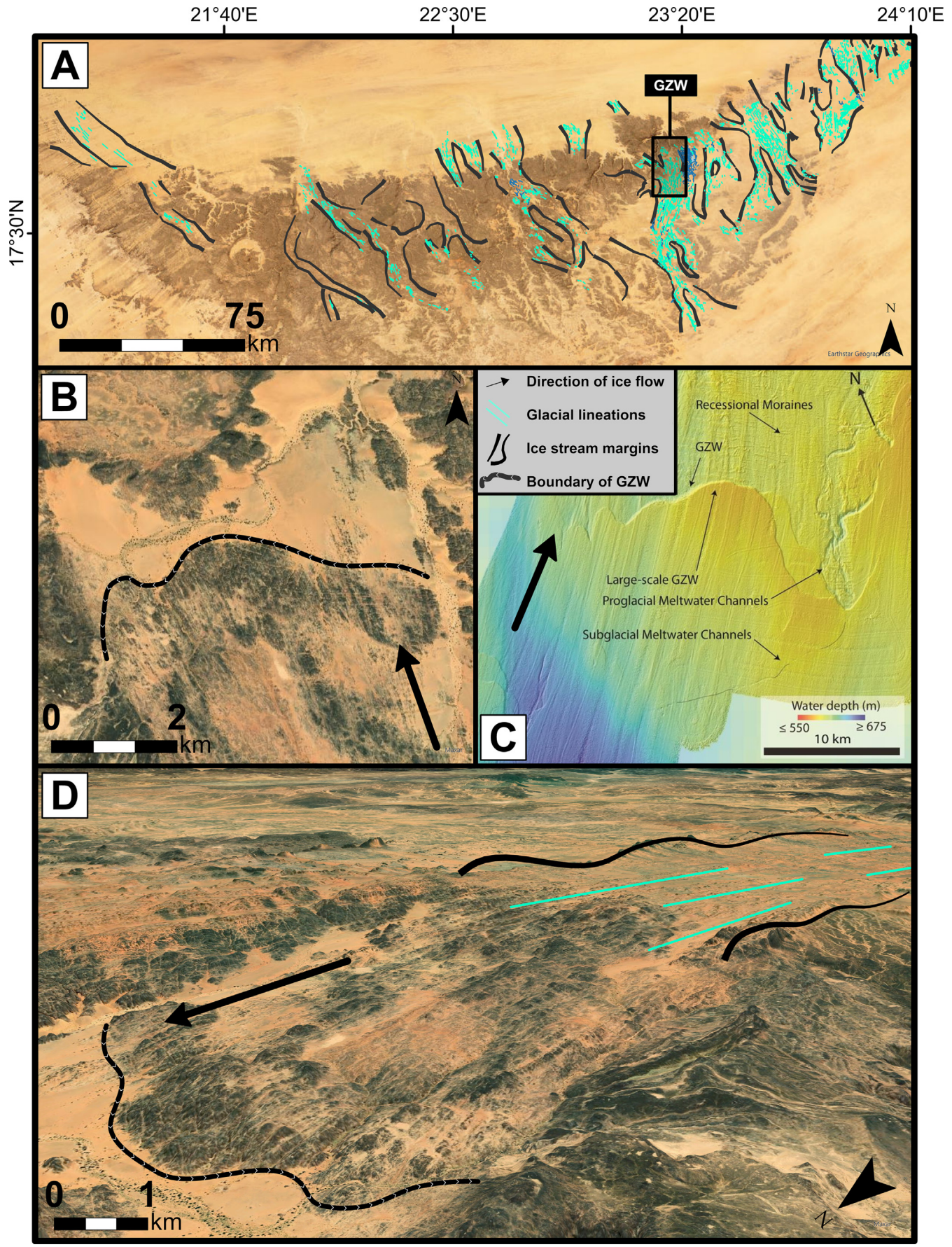
21°40'E
22°30'E
23°20'E
24°10'E
17°30'N
A
GZW
0
75
km
N
Earthstar Geographics
B
0
2
km
Direction of ice flow
Glacial lineations
Ice stream margins
Boundary of GZW
Recessional Moraines
GZW
Large-scale GZW
Proglacial Meltwater Channels
Subglacial Meltwater Channels
Water depth (m)
≤ 550
≥ 675
10 km
C
D
0
1
km

(Batchelor and Dowdeswell, 2015; Dowdeswell et al., 2020). Here, meltwater-transported debris can be deposited from deforming sedimentary beds beneath fast-flowing ice streams during still-stands in ice-sheet retreat. The measurements of the proposed GZW in the Ennedi are consistent with data from modern high-latitude GZWs, which are generally <15 km long, between 4 and 280 km wide, and 15 to 100 m thick (Batchelor and Dowdeswell, 2015).

Although interpretations of pre-Cenozoic GZWs have been attempted from a purely sedimentological perspective (Dietrich and Hofmann, 2019; Le Heron et al., 2022), no geomorphological evidence for these has been published. Therefore, in this study, we present the first geomorphological description of an exposed GZW in association with large-scale glacial lineations situated at the margin of an ice stream.

4.4. Anatomy of a palaeo-channel system in inverted relief

The discovery of inverted palaeo-channels in close proximity to large-scale glacial lineations in the Ennedi raises several questions (Kettler et al., this issue). These revolve around the multiple generations of channels that one can interpret on the basis of true-colour imagery, and thus the related issue of the number of sedimentary cycles that can be preserved. Therefore, we have adopted band-ratioing and the PCA technique (Principal Component Analysis) in order to interpret the geometry, mineralogical differences and cross-cutting features, and showcase this here in several examples.

The ICA (Inverted Channel Assemblage) is composed of N-NNW oriented inverted palaeo-channels within Ice Stream VII, surrounded by large-scale glacial lineations of ice streams VI and VIII (Fig. 8A). Most ridges have a width between ~100 and 500 m (Kettler et al., this issue). Additionally, the quality of preservation varies significantly with channels on different topographic levels. Typical sinuosities range between 1.01 and 1.2 (Table 2), but in general sinuosity is low with values <1.05. Specific sinuosity ranges are not a unique feature of palaeo-channels and can therefore not be used as clear evidence for fluvial or glaciofluvial activity (Butcher et al., 2021). Owing to the effects of diagenesis, weathering, and partial concealment by Quaternary sediment, it is important to recognise that the dimensions of the exhumed ridges may not exactly mirror the original channel dimensions. Therefore, the sinuosity and the length of the ridges can only be regarded as estimates for the original channel geometry. The ridge length is partly obscured by extensive weathering and sand cover, but the longest ridge (#21, Fig. 8B) is about 10 km. Measurements were taken along the crestline wherever possible. The ridges have been re-classified into six groups (Fig. 8D) based on visual interpretation instead of three as proposed by Kettler et al. (issue). Criteria for the following categorisation are: state of preservation, crosscutting relationships, connectivity of ridge parts, dissection of other glacial features and surface mineralogy. Note that the grouping does not suggest a possible chronological sequence and is an extension of the classification into three groups from Kettler et al. (this issue). Group 1 deals with isolated remnants of former channels that do not show a continuous connection between their respective parts and are typically less than a kilometre long. Ridges of groups 2 and 3 (#16,17,20) show signs of pronounced weathering and erosion. Sand cover obscures most of the surfaces and does not allow for a reasonable surface mineral identification or differentiation of individual channels. Overall sinuosity lies between 1.099 and 1.351, whilst the ridge length ranges from ~1300 m to ~4300 m. Group 4 (#2, 3, 4, 5, 6, 7, 8) comprises ridges of the central and western area with a higher level of preservation than groups 1–3. Ridge lengths are between ~1700 m and ~6600 m and sinuosity ranges from 1.010 to 1.257. Ridges from this group along with those of groups 3 and 5 amalgamate with one another in the northern part. Group 5 (#9, 10, 11, 12, 13, 14, 15, 18, 19) contains ridges with clear boundaries and distinct bends. Their state of preservation is the highest amongst the former groups and along with group 6 (#21) they comprise the uppermost channels. #21 (group 6) is the longest almost continuous ridge, at ~10 km. The general orientation is to the north (NNW-NNE) with one ridge oriented to the NE (37°). Cross-cutting and vertical stacking of ridges can best be observed at seven prominent locations (crosscutting sections, CCS; Fig. 9) and attests to an evolution of the system in time and space. The band-ratio technique allows a more detailed differentiation of the individual ridges and offers a general overview of the differences in the mineral composition of the surface (Fig. 9C and F).

We interpret the assemblage of inverted channel sediments as a proglacial sandur setting (Kettler et al., this issue). The crosscutting relationships demonstrate the occurrence of multiple generations of channels that were cut into the sediment during meltwater release at the glacier front.

Other examples of exhumed ridges are distributed over Ice Streams V, VI and X. These occur as single strands or in clusters. However, they are less convincing in their morphology and have not been studied further.

5. Discussion

Published evidence for glacial features younger than Ordovician age in the Ennedi Plateau is completely lacking (Ghienne et al., 2023). This paper presents a unique and excellently preserved area where glacial activity during the LPIA has shaped and transformed the landscape.

5.1. Marine-terminating ice sheet

The Ennedi Plateau offers one of the most convincing assemblages of palaeo-ice sheet geomorphological features in the late Palaeozoic record (Le Heron, 2018; Kettler et al., this issue). Large discrete ice-stream pathways separated by interstream areas extend across the entire plateau and preserve a comprehensive collection of glacial landforms, such as large-scale lineations, striated surfaces, sharp lateral boundaries, exhumed former channel sediments, and a GZW. The occurrence of marine sediments on the northern margin of the Ennedi Plateau in the Mourdi Depression (Mahamoud, 1986; Klitzsch et al., 1993) allowed Torsvik and Cocks (2011, 2013) to illustrate the approximate reconstruction of the coastline during the Carboniferous in northern Africa. It is further evident from the spatial distribution of ice streams that the Ennedi ice sheet flowed northwards, thus perpendicular to this proposed E-W striking shoreline. The GZW described herein provides a vital piece of evidence that underpins the proposed coastal geometry during the LPIA. This interpretation is based on the composition, shape, and thickness of the GZW, and moreover its relationship with surrounding glacial features. Specifically, the Ennedi GZW has a shallow ice-proximal side and a steeper ice-distal side consistent with the general direction of ice flow. Glacial lineations appear to be present on top of the GZW. This might attest to a re-advance of the ice stream after the deposition of the GZW material. Interpretations of GZWs in the ancient geological record are rare (Dietrich and Hofmann, 2019). Modern examples, on the other hand, are quite common (Batchelor and Dowdeswell, 2015; Dowdeswell et al., 2016; Fig. 7). Given its location, the Ennedi GZW is postulated to represent a transition from ice stream to floating ice during ice still-stand as part of an overall retreat

Fig. 7. (A) Location of the grounding zone wedge (GZW) on Ice Stream VI. (B) Close-up view on the GZW (coordinates: 17°45′21.5″N 23°16′36.8″E). (C) GZW from Antarctica as a comparison to the Ennedi GZW (Image modified from Demet, 2016). (D) ArcGIS Pro: oblique view, vertical exaggeration: 5×.

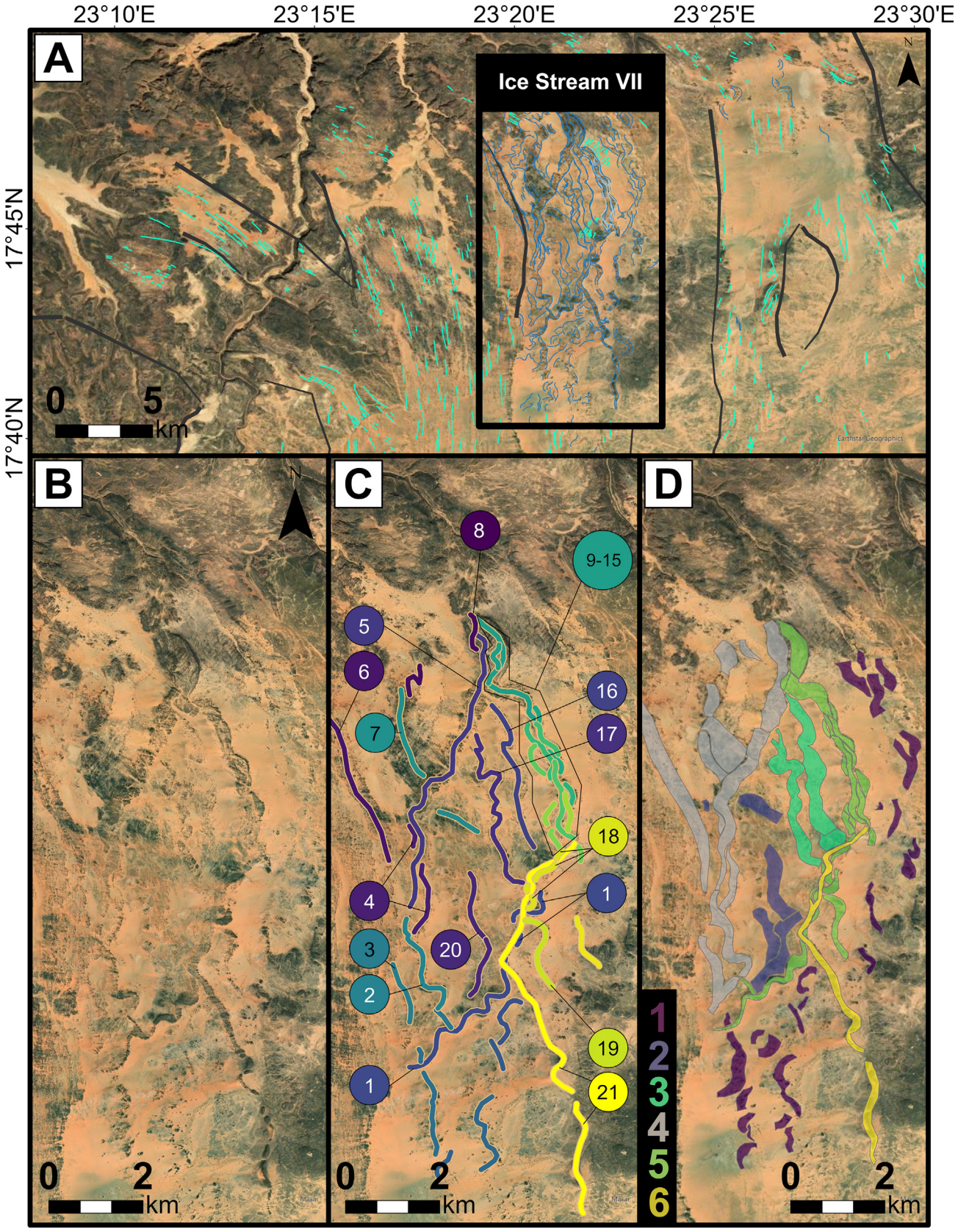

Fig. 8. (A) Location of the 'Inverted Channel Assemblage' (ICA); (B) satellite image of the ICA (coordinates: 17°45′22.5″N 23°21′00.9″E); (C) the most prominent channels are marked and numbered (Table 1); (D) ridges are grouped based on the criteria in Section 4.4 (for additional details see also Figs. 3 and 4 in Kettler et al., this issue).

Table 2
Measurements of ridges in the "Inverted Channel Assemblage" (ICA).

#*a	Ridge length [m]*b	Length of straight line [m]*c	Sinuosity*d	Elevation start [hm]*e	Elevation end [hm]*f	Difference elevation start–end [m]*g	Orientation [°]/direction	Group
1	6545	5017	1.304	997	983	14	37/NE	5
2	2714	2158	1.257	1002	1007	−5	341/NNW	4
3	1368	1321	1.035	1002	1004	−2	344/NNW	2
4	2607	2438	1.069	997	992	5	358/N	4
5	6645	6039	1.100	998	979	19	15/NNE	4
6	4695	4647	1.010	998	980	18	336/NNW	4
7	2034	1957	1.039	971	970	1	346/NNW	4
8	1694	1542	1.098	945	931	14	356/N	4
9	1575	1324	1.189	987	982	5	307/NW	5
10	352	334	1.053	987	977	10	346/NNW	5
11	3497	2866	1.220	987	986	1	350/N	5
12	2569	2181	1.177	980	986	−6	–	5
13	611	544	1.123	976	979	−3	330/NNW	5
14	844	800	1.055	981	985	−4	355/N	5
15	367	328	1.118	975	978	−3	352/N	5
16	3668	3302	1.110	990	978	12	345/NNW	3
17	4356	3222	1.351	995	970	25	344/NNW	3
18	1768	1518	1.164	993	985	8	30/NNE	5
19	1969	1625	1.043	981	996	−15	339/NNW	5
20	2875	2617	1.099	1001	999	2	3/N	2
21	10,185	8414	1.210	987	980	7	358/N	6

This table shows measurements for prominent ridges. *a: The ridge number can be seen in Fig. 8C; *b: Ridge length in total [m] includes the whole ridge but in some cases, it is not clear where one ridge begins and the other ends. *c: Length of straight line refers to the direct (straight) path between the visible start and end of the ridge; *d: Sinuosity is the length of the ridge divided by the length of the straight line between start and end. *e–f: 'Elevation start' is the most southern point still visible, 'elevation end' is the most northern point of a specific ridge; *g: Difference in elevation from start to end is negative if the end point is higher above the ground than the starting point.

phase. Internally, therefore, the GZW might contain evidence for erosional channels and sorted sediments but this remains to be tested through fieldwork.

5.2. Expansion of the Ennedi ice sheet

An accumulation of palaeo-ice stream pathways with various glacial features was identified on the Devonian surface of the Ennedi Plateau (Fig. 1D; Fig. 2). Newly discovered features in the NW area of the Ennedi give rise to the assumption that the ice sheet was even larger than described in Le Heron (2018) and Kettler et al. (this issue). One additional ice stream (Ice Stream I) to add to the collection that started with Le Heron (2018) and Kettler et al. (this issue) is proposed which expands the area of ice influence on the Ennedi Plateau. Two generations of large-scale parallel lineations on two discrete stratigraphic levels to the NW and SE of a wedge provide evidence of multiple different phases of ice recession/advance with several tens of metres of sediment in between representing the stratigraphic archive of these cycles (Fig. 4). One of the advantages of the Ennedi successions is the composition with relatively undeformed sedimentary rocks. These conditions are ideal for the recognition of ancient surface structures such as subglacial bedforms. Furthermore, the absence of later orogenic deformation means that structures such as cleavage or foliations can be readily dismissed. In a highly similar geological context, the sandstones of the Tassili' n'Ajjer plateau straddling the Algerian and Libyan border have excellent glacial lineations that are readily observed from satellite imagery (Moreau et al., 2005). This plateau is also undeformed and has been extensively investigated in terms of field research from multiple different teams to interpret the Late Ordovician glacial record. Collectively therefore these examples serve as excellent precedence for the large-scale interpretation of the Ennedi Plateau.

5.3. Soft-sediment striated surfaces

In recent years, there has been an attempt to fully exploit the power of satellite images in the interpretation of palaeo-glacial landscapes and geomorphology in the deep time record. As summarised by Le Heron et al. (2022) a significant risk factor in this approach, where ground truthing/fieldwork is not done in parallel, is the misinterpretation of other non-glacial geomorphological or geomorphological structures as having a glacial origin. This is particularly an issue in parts of Gondwana where metasediments deformed during the complex Pan African-Brasiliano Orogeny occur, such as in the Damara Belt of Namibia (Andrews et al., 2019). Consequently, the evidence for soft-sediment striated surfaces at outcrop in the Ennedi significantly strengthens the overall interpretation of a palaeo-ice stream sediment landform assemblage. In the Late Ordovician, by comparison, the glacial record is dominantly sandy in Morocco to Saudi Arabia, the explanation for which is commonly a long hiatus prior to glaciation in conjunction with multiple generations of sediment cannibalisation and recycling (e.g. Meinhold et al., 2021). In the Ennedi, the overall context during the LPIA therefore appears to be a shallow, gently dipping shelf with strong parallels with the early Palaeozoic shelf system of northern Gondwana (Ghienne et al., 2014). According to Klitzsch et al. (1993), the Devonian record of the Ennedi – in which the glacial record is developed – comprises mainly clayey to fine- and medium-sand shallow marine deposits with fluviatile sediments visible as ridges (see also Fig. 3 in Klitzsch et al., 1993). We propose that prior to the glaciation of the Ennedi Plateau during the LPIA, sediment recycling occurred in a marine basin that was already present in the Silurian. During the Devonian, shallow transgressions occurred over a broad shelf area, leaving reworked sediments supplemented by fluviatile input to the south (Klitzsch et al., 1993; Aubert et al., 2013) in which the soft-sediment striations could have developed. Given the context in the Ennedi, it remains an open question whether the soft-sediment striated surfaces could represent a previously considered small-scale endmember of the continuum of subglacial bedforms proposed in Ely et al. (2016).

5.4. Meltwater channel sediments

Application of band-ratioing of the satellite image date in concert with principal component analysis permits significant new insights into the inverted channel assemblage (ICA) of the Ennedi which is proposed to represent a proglacial sandur setting (Kettler et al., this issue). To the author's knowledge, no comparable system of inverted palaeochannels is known from the LPIA record outside of Chad, with the exception of an interpreted tunnel valley system in the Paraná Basin (Brasil; Vesely et al., 2021). Furthermore, inverted sinuous ridges in the

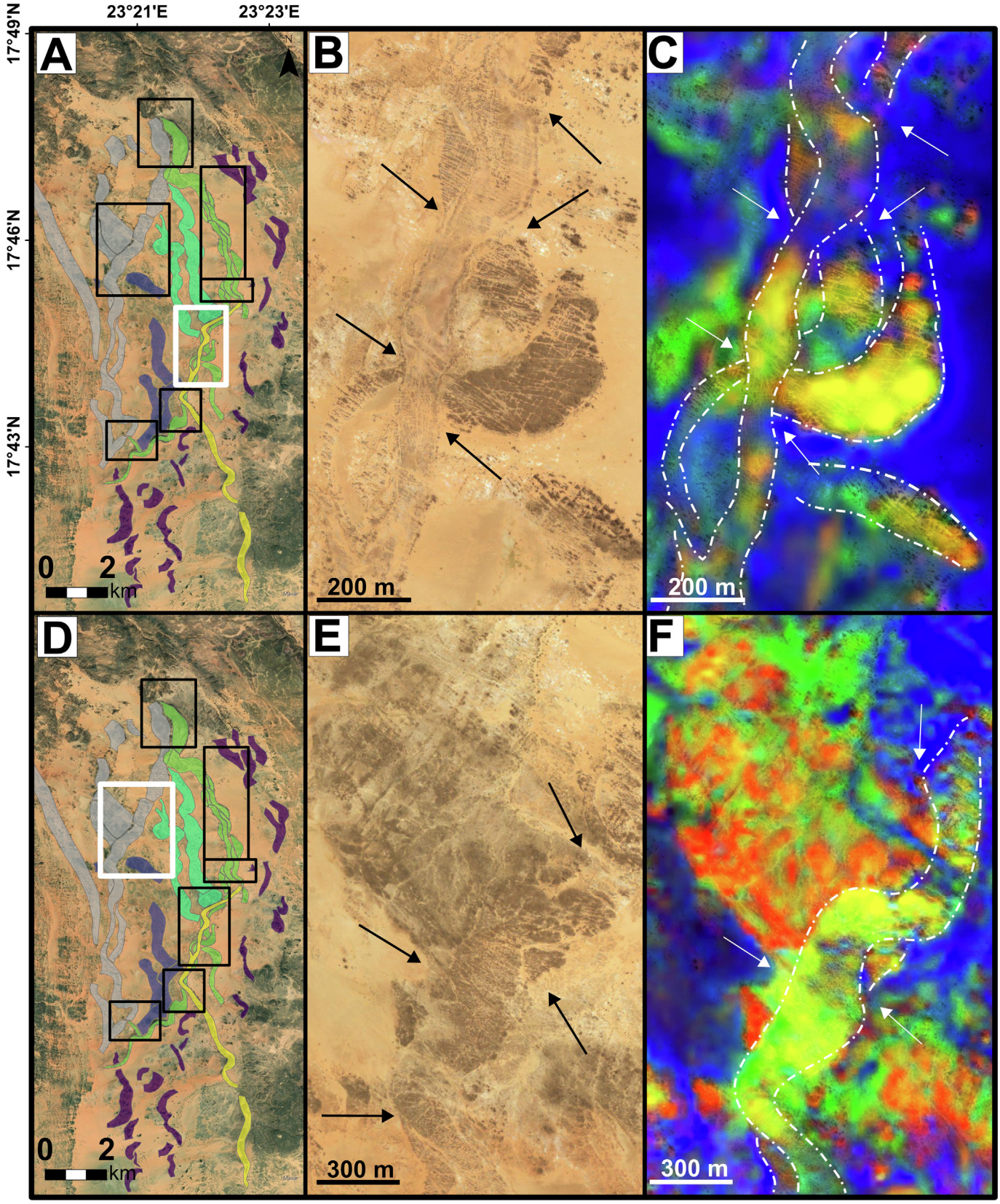

Fig. 9. Two examples for crosscutting sections (CCS) in the ICA; (A) the CCS are marked with rectangles. The white box shows the location of (B) and (C); (B) CCS with arrows pointing to channels on different topographic levels; (C) image from (B) with Landsat-8 FCC overlay (R: 7/5 + 3/4; G: 6/7; B: 4/3; centre coordinates: 17°44′29.0″N 23°21′57.7″E); (D) The white box shows the location of (E) and (F); (E) Channel #5 cuts through a wide ridge-like structure. (F) Differences in surface mineralogy are visible and distinguish the channel material from the underlying sediment and the sand cover (coordinates: 17°45′45.0″N 23°20′42.8″E).

palaeo-record of fluvial and glaciofluvial origin can be seen worldwide and on Mars (Butcher et al., 2021; Zaki et al., 2021). Crosscutting relationships allow the build-up of a tentative chronology which speaks either for (i) waxing and waning of the ice sheet/ice stream followed by an interglacial episode during which the channel material was overlain by sediment and thus preserved, or (ii) the successive deposition of channel material in multiple episodes of meltwater release during glacial retreat. Whether this chronology relates to discrete avulsion phases or separate glacial cycles remains to be tested with field work.

Migration, avulsion, and aggradation are reflected by sets of channel bars and fills. These deposits do not reflect the original width of the channels. Multiple levels of stacked channel material are typically formed by lateral accretion of rivers migrating over the outwash plain/floodplain (Marren, 2005). Kettler et al. (this issue) propose a proglacial sandur area as an explanation for the distribution of the ridges and channel bodies, which formed during ice sheet retreat and enhanced meltwater production. Preservation variability, crosscutting relationships, and their occurrence at different topographic levels, suggest that these are diachronous features documenting sequential stages of deglaciation. As can be seen in recent examples, such as Iceland (e.g. Marren, 2002) or the Patagonian Icefield (Davies et al., 2020), areas of meltwater activity can be reshaped repeatedly during successive cycles. Only the last episode of meltwater release will be preserved, followed by possible fluvial activity with no glacial influence. Based on the currently available data, two possible end scenarios for the emergence of the proglacial sandur system are proposed: (i) A single retreat cycle of Ice Stream VII could have produced a series of events with significant meltwater release, followed by rapid burial. (ii) Separate phases of ice sheet recessions produced different successions of meltwater release that were subsequently overprinted and/or supplemented by the discharge of sufficient meltwater in the following ice sheet retreat event.

It is emphasised that the analysis herein, and hypotheses developed from it, will require additional ground truthing and collection of field samples.

6. Conclusions

Satellite image data analysis techniques provide a major step forward in the interpretation of glacial environments of the late Palaeozoic on the Ennedi Plateau. This approach allows for the study of the glacial features in far greater depth than previously attempted (Le Heron, 2018; Kettler et al., this issue). Since the discovery of the Ennedi ice sheet, the area has not only been significantly expanded (Kettler et al., this issue; this study), but numerous newly found structures, such as a GZW or soft-sediment striated surfaces, allow for an increasingly detailed insight into the development of a late Palaeozoic ice mass. We list the following highlights as important:

- The discovery of a new palaeo-ice stream (Ice Stream I) in the western part of the plateau increases the general area of known glaciation to a total of ten prominent palaeo-ice stream pathways. Furthermore, at least two generations of glacial lineations separated by a sediment wedge on Ice Stream I show that the ice sheet moved through different phases of waxing and waning with tens of metres of sediment deposition between these phases.
- Soft-sediment striated surfaces (Ice Stream V), which are parallel to ice flow mapped on satellite imagery, support the argument of subglacial shearing.
- A GZW (Ice Stream VI) adds to the evidence of a marine-terminating ice sheet.
- Band-ratioing and the PCA technique expand the range of data that can be obtained from satellite imagery and allow the presentation of a more comprehensive picture of the temporal and spatial development of the inverted channels based on clear differences in geometry, preservation, crosscutting features and surface mineralogy.

Overall, the Ennedi Plateau offers an excellent insight into the history of a vast palaeo-ice sheet during the LPIA with an extensive range of glacial structures in excellent condition of preservation that is unique in the palaeo-record of the Palaeozoic.

Data availability

Data will be made available on request.

Declaration of competing interest

The authors declare that they have no known competing financial interests that could have appeared to influence the work reported in this paper.

Acknowledgements

The authors wish to thank the reviewers, Eduardo Menozzo Da Rosa and Neil Griffis, for extremely useful input which helped improve the quality of the work. We also thank the editors, Fernando Vesely and Massimo Moretti, for their input and handling the paper. RW acknowledges funding through a University of Vienna PraeDoc scholarship.

References

Andrews, G.D., McGrady, A.T., Brown, S.R., Maynard, S.M., 2019. First description of subglacial megalineations from the late Paleozoic ice age in southern Africa. PLoS One 14, e0210673. https://doi.org/10.1371/journal.pone.0210673.

Askari, G., Pour, A.B., Pradhan, B., Sarfi, M., Nazemnejad, F., 2018. Band Ratios Matrix Transformation (BRMT): a sedimentary lithology mapping approach using ASTER satellite sensor. Sensors 18, 3213. https://doi.org/10.3390/s18103213.

Aubert, M., Kraiem, A., Haeberlin, Y., Zwahlen, F., 2013. From satellite imagery to hydrogeological survey maps of Chad – 2013. 11th Swiss Geoscience Meeting, Lausanne November 2012 . https://docplayer.fr/81724468-Presentations-des-resultats-du-projet-reseau.html. (Accessed 11 July 2023).

Batchelor, C.L., Dowdeswell, J.A., 2015. Ice-sheet grounding-zone wedges (GZWs) on high-latitude continental margins. Marine Geology 363, 65–92. https://doi.org/10.1016/j.margeo.2015.02.001.

Brugière, D., Scholte, P., 2013. Biodiversity gap analysis of the protected area system in poorly-documented Chad. Journal for Nature Conservation 21, 286–293. https://doi.org/10.1016/j.jnc.2013.02.004.

Bussert, R., 2010. Exhumed erosional landforms of the Late Palaeozoic glaciation in northern Ethiopia: indicators of ice-flow direction, palaeolandscape and regional ice dynamics. Gondwana Research 18, 356–369. https://doi.org/10.1016/j.gr.2009.10.009.

Butcher, F.E.G., Balme, M.R., Conway, S.J., Gallagher, C., Arnold, N.S., Storrar, R.D., Lewis, S.R., Hagermann, A., Davis, J.M., 2021. Sinuous ridges in Chukhung crater, Tempe Terra, Mars: implications for fluvial, glacial, and glaciofluvial activity. Icarus 357, 114131. https://doi.org/10.1016/j.icarus.2020.114131.

Canals, M., Amblas, D., 2016. The bundle: mega-scale glacial landform left by an ice stream, Western Bransfield Basin. In: Dowdeswell, J.A., Canals, M., Jakobsson, M., Todd, B.J., Dowdeswell, E.K., Hogan, K.A. (Eds.), Atlas of Submarine Glacial Landforms: Modern, Quaternary and Ancient. Geological Society of London, Memoirs46, pp. 177–178. https://doi.org/10.1144/M46.157.

Davies, B.J., Darvill, C.M., Lovell, H., Bendle, J.M., Dowdeswell, J.A., Fabel, D., García, J.-L., Geiger, A., Glasser, N.F., Gheorghiu, D.M., Harrison, S., Hein, A.S., Kaplan, M.R., Martin, J.R.V., Mendelova, M., Palmer, A., Pelto, M., Rodés, Á., Sagredo, E.A., Smedley, R.K., Smellie, J. L., Thorndycraft, V.R., 2020. The evolution of the Patagonian Ice Sheet from 35 ka to the present day (PATICE). Earth-Science Reviews 204, 103152. https://doi.org/10.1016/j.earscirev.2020.103152.

Demet, B.P., 2016. Sedimentary Processes at Ice Sheet Grounding-zone Wedges: Comparing Planform Morphology From the Western Ross Sea (Antarctica) to Internal Stratigraphy From Outcrops of the Puget Lowlands (Washington State, U.S.A.). (M.Sc. Thesis)Rice University, Houston, Texas USA.

Demet, B.P., Nittrouer, J.A., Anderson, J.B., Simkins, L.M., 2018. Sedimentary processes at ice sheet grounding-zone wedges revealed by outcrops, Washington State (USA). Earth Surface Processes and Landforms 2019 (44), 1209–1220. https://doi.org/10.1002/esp.4550.

Deynoux, M., Ghienne, J.-F., 2004. Late Ordovician glacial pavements revisited: a reappraisal of the origin of striated surfaces. Terra Nova 16, 95–101. https://doi.org/10.1111/j.1365-3121.2004.00536.x.

Dietrich, P., Hofmann, A., 2019. Ice-margin fluctuation sequences and grounding zone wedges: the record of the Late Palaeozoic Ice Age in the eastern Karoo Basin (Dwyka Group, South Africa). The Depositional Record 5, 247–271. https://doi.org/10.1002/dep2.74.

Domeier, M., Torsvik, T.H., 2014. Plate tectonics in the late Paleozoic. Geoscience Frontiers 5 (3), 303–350. https://doi.org/10.1016/j.gsf.2014.01.002.

Dowdeswell, J.A., Fugelli, E.M.G., 2012. The seismic architecture and geometry of grounding-zone wedges formed at the marine margins of past ice sheets. GSA Bulletin 123, 1750–1761. https://doi.org/10.1130/B30628.1.
Dowdeswell, J.A., Ottesen, D., Forwick, M., 2016. Grounding-zone wedges on the western Svalbard shelf. In: Dowdeswell, J.A., Canals, M., Jakobsson, M., Todd, B.J., Dowdeswell, E.K., Hogan, K.A. (Eds.), Atlas of Submarine Glacial Landforms: Modern, Quaternary and Ancient. Geological Society of London, Memoirs46, pp. 233–234. https://doi.org/10.1144/M46.128.
Dowdeswell, J.A., Batchelor, C.L., Montelli, A., Ottesen, D., Christie, F.D.W., Dowdeswell, E.K., Evans, J., 2020. Delicate seafloor landforms reveal past Antarctic grounding-line retreat of kilometers per year. Science 368, 1020–1024. https://doi.org/10.1126/science.aaz3059.
Earth Explorer, USGS, d. https://earthexplorer.usgs.gov/. (Accessed 3 July 2023).
Ely, J., Clark, C.D., Spagnolo, M., Stokes, C.R., Greenwood, S.L., Hughes, A.L.C., Dunlop, P., Hess, D., 2016. Do subglacial bedforms comprise a size and shape continuum. Geomorphology 257, 108–119. https://doi.org/10.1016/j.geomorph.2016.01.001.
Fielding, C.R., Frank, T.D., Birgenheier, L.P., 2023. A revised, late Palaeozoic glacial time-space framework for eastern Australia, and comparisons with other regions and events. Earth-Science Reviews 236, 104263. https://doi.org/10.1016/j.earscirev.2022.104263.
Ghienne, J.-F., Desrochers, A., Vandenbroucke, T.R.A., Achab, A., Asselin, E., Dabard, M.-P., Farley, C., Loi, A., Paris, F., Wickson, S., Veizer, J., 2014. A Cenozoic-style scenario for the end-Ordovician glaciation. Nature Communications 5, 4485. https://doi.org/10.1038/ncomms5485.
Ghienne, J.-F., Moussa, A., Saad, A., Djatibeye, B., Youssou, H.M., 2023. The Ordovician strata of the Ennedi Plateau, northeastern Chad (Erdi Basin). Comptes Rendus Géoscience 355, 63–84. https://doi.org/10.5802/crgeos.180.
Gindre, L., Le Heron, D., Bjørnseth, H.M., 2012. High resolution facies analysis and sequence stratigraphy of the Siluro-Devonian succession of Al Kufrah basin (SE Libya). Journal of African Earth Sciences 76, 8–26. https://doi.org/10.1016/j.jafrearsci.2012.08.002.
Goldthwait, R.P., 1979. Giant grooves made by concentrated basal ice streams. Journal of Glaciology 23, 297–307. https://doi.org/10.3189/S0022143000029919.
Griffis, N., Montañez, I.P., Mundil, R., Le Heron, D.P., Dietrich, P., Kettler, C., Linol, B., Mottin, T., Vesely, F., Iannuzzi, R., Huyskens, M., Yin, Q.-Z., 2021. High-latitude ice and climate control on sediment supply across SW Gondwana during the late Carboniferous and early Permian. GSA Bulletin 133, 2113–2124. https://doi.org/10.1130/B35852.1.
Haeberlin, Y., Kraiem-Morard, A., Aubert, M., Zwahlen, F., Bünzli, M.-A., Mohammed, I.M., Sénégas, O., Guidotti, G., 2016. Conception et méthodes appliquées à l'élaboration des cartes hydrogéologiques au 1:500 000 et 1:200 000 des régions nord et est du. http://reseau-tchad.org/cdig/media/SIRE_Biblio/Publications/Hydrogeologie/DocTec_N1_Concept_methodes_2016-04.pdf (in French).
Isbell, J.L., Henry, L.C., Gulbranson, E.L., Limarino, C.O., Fraiser, M.L., Koch, Z.J., Ciccioli, P.L., Dineen, A.A., 2012. Glacial paradoxes during the late Paleozoic ice age: evaluating the equilibrium line altitude as a control on glaciation. Gondwana Research 22, 1–19. https://doi.org/10.1016/j.gr.2011.11.005.
Isbell, J.L., Fedorchuk, N.D., Rosa, E.L.M., Goso, C., Alonso-Muruaga, P.J., 2023. Reassessing a glacial landscape developed during terminal glaciation of the Late Paleozoic Ice Age in Uruguay. Sedimentary Geology 451. https://doi.org/10.1016/j.sedgeo.2023.106399.
Jakobsson, M., Anderson, J.B., 2016. Corrugation ridges in the Pine Island Bay glacier trough, West Antarctica. Geological Society, London, Memoirs 46, 265–266. https://doi.org/10.1144/M46.5.
Jakobsson, M., Polyak, L., Edwards, M., Kleman, J., Coakley, B., 2008. Glacial geomorphology of the Central Arctic Ocean: the Chukchi Borderland and the Lomonosov Ridge. Earth Surface Processes and Landforms 33, 526–545. https://doi.org/10.1002/esp.1667.
Kettler, C., Wohlschlägl, R., Russel, C., Scharfenberg, L., Ghienne, J.-F., Le Heron, D.P., 2023. A World-class Example of a Late Palaeozoic Glaciated Landscape in Chad (this issue).
Klitzsch, E., 1983. Paleozoic formations and a Carboniferous glaciation form the Gilf Kebir-Abu Ras Area in southwestern Egypt. Journal of African Earth Sciences 1, 17–19.
Klitzsch, E., Reynolds, P.-O., Barazi, N., 1993. Geologische Erkundungsfahrt zum Ostteil des Ennedi Gebirges und der Mourdi Depression (NE Sudan) im Januar 1992. Würzburger Geographische Arbeiten 87, 49–61 (in German).
Lang, J., Yahaya, M., El Hamet, M.O., Besombes, J.C., Cazoulat, M., 1991. Depôts glaciaires du Carbonifere inférieur a l'Ouest de l'Air (Niger). Geologische Rundschau 80, 611–622. https://doi.org/10.1007/BF01803689 (in French).
Lawver, L.A., Dalziel, I.W.D., Norton, I.O., Gahagan, L.M., Davis, J.K., 2014. The PLATES 2014 Atlas of Plate Reconstructions (550 Ma to Present Day), PLATES Progress Report No. 374-2015. No. 201. University of Texas Technical Report, p. 220.
Le Heron, D.P., 2018. An exhumed Paleozoic glacial landscape in Chad. Geology 46, 91–94. https://doi.org/10.1130/G39510.1.
Le Heron, D.P., Sutcliffe, O.E., Whittington, R.J., Craig, J., 2005. The origins of glacially related soft-sediment deformation structures in Upper Ordovician glaciogenic rocks: implication for ice-sheet dynamics. PALAEO 218, 75–103. https://doi.org/10.1016/j.palaeo.2004.12.007.
Le Heron, D.P., Armstrong, H.A., Wilson, C., Howard, J.P., Grinder, L., 2010. Glaciation and deglaciation of the Libyan Desert: the Late Ordovician record. Sedimentary Geology 223, 100–125. https://doi.org/10.1016/j.sedgeo.2009.11.002.
Le Heron, D.P., Meinhold, G., Elgadry, M., Abutarruma, Y., Boote, D., 2014. Early Palaeozoic evolution of Libya: perspectives from Jabal Eghei with implications for hydrocarbon exploration in Al Kufrah Basin. Basin Research 27, 60–83. https://doi.org/10.1111/bre.12057.
Le Heron, D.P., Dietrich, P., Busfield, M.E., Kettler, C., Bermanschläger, S., Grasemann, B., 2019. Scratching the surface: footprint of a late Carboniferous ice sheet. Geology 47, 1034–1038. https://doi.org/10.1130/G46590.1.
Le Heron, D.P., Heninger, M., Baal, C., Bestmann, M., 2020. Sediment deformation and production beneath soft-bedded Palaeozoic ice sheets. Sedimentary Geology 408, 105761. https://doi.org/10.1016/j.sedgeo.2020.105761.
Le Heron, D.P., Kettler, C., Griffis, N.P., Dietrich, P., Montañez, I.P., Osleger, D.A., Hofmann, A., Douillet, G., Mundil, R., 2021. The Late Palaeozoic Ice Age unconformity in southern Namibia viewed as a patchwork mosaic. The Depositional Record 8, 419–435. https://doi.org/10.1002/dep2.163.
Le Heron, D.P., Busfield, M.E., Chen, X., Corkeron, M., Davies, B.J., Dietrich, P., Ghienne, J.-F., Kettler, C., Scharfenberg, L., Vandyk, T.M., Wohlschlägl, R., 2022. New perspectives on glacial geomorphology in Earth's deep time record. Frontiers in Earth Science 10. https://doi.org/10.3389/feart.2022.870359.
Limarino, C.O., López-Gamundí, O.R., 2021. Late Paleozoic basins of South America: insights and progress in the last decade. Journal of South American Earth Sciences 107, 103150. https://doi.org/10.1016/j.jsames.2020.103150.
Liu, J.G., Mason, P.J., 2016. Image Processing and GIS for Remote Sensing: Techniques and Applications. John Wiley & Sons, Ltd., West Sussex, PO19 8SQ, UK (457 pp.).
Lüning, S., Craig, J., Fitches, B., Mayouf, J., Busrewil, A., El Dieb, M., Gammudi, A., Loydell, D., McIlroy, D., 1999. Re-evaluation of the petroleum potential of the Kufra Basin (SE Libya, ne Chad): does the source rock barrier fall? Marine and Petroleum Geology 16, 693–718. https://doi.org/10.1016/S0264-8172(99)00013-6.
Mahamoud, A.H., 1986. Geologie und Hydrogeologie des Erdis-Beckens, NE-Tschad. Berliner Geowissensch. Abh. A76 p. 67 (in German).
Marren, P.M., 2002. Glacier margin fluctuations, Skaftafellsjökull, Iceland: implications for Sandur evolution. Boreas 31, 75–81. https://doi.org/10.1111/j.1502-3885.2002.tb01057.x.
Marren, P.M., 2005. Magnitude and frequency in proglacial rivers: a geomorphological and sedimentological perspective. Earth-Science Reviews 70, 203–251. https://doi.org/10.1016/j.earscirev.2004.12.002.
Meinhold, G., Bassis, A., Hinderer, M., Lewin, A., Berndt, J., 2021. Detrital zircon provenance of North Gondwana Palaeozoic sandstones from Saudi Arabia. Geological Magazine 158, 442–458. https://doi.org/10.1017/S0016756820000576.
Montañez, I.P., 2022. Current synthesis of the penultimate icehouse and its imprint on the Upper Devonian through Permian stratigraphic record. In: Lucas, S.G., Schneider, J.W., Wang, X., Nikolaeva, S. (Eds.), The Carboniferous Timescale. Geological Society of London, Special Publications512, pp. 213–245. https://doi.org/10.1144/SP512-2021-124.
Montañez, I.P., Poulsen, C.J., 2013. The Late Paleozoic Ice Age: an evolving paradigm. Annual Review of Earth and Planetary Sciences 41, 629–656. https://doi.org/10.1146/annurev.earth.031208.100118.
Moreau, J., Ghienne, J.-F., Le Heron, D., Rubino, J.-L., Deynoux, M., 2005. A 440 Ma old ice stream in North Africa. Geology 33, 753–756. https://doi.org/10.1130/G21782.1.
Munro-Stasiuk, M.J., Fisher, T.G., Nitzsche, C.R., 2005. The origin of the western Lake Erie grooves, Ohio: implications for reconstructing the subglacial hydrology of the Great Lakes sector of the Laurentide Ice Sheet. Quaternary Science Reviews 24, 2392–2409. https://doi.org/10.1016/j.quascirev.2004.11.018.
Osinowo, O.O., Gomy, A., Isseini, M., 2021. Mapping hydrothermal alteration mineral deposits from Landsat 8 satellite data in Pala, Mayo Kebbi Region, Southwestern Chad. Scientific African 11, e00687. https://doi.org/10.1016/j.sciaf.2020.e00687.
Richards, J.A., Jia, X., 2006. Remote Sensing Digital Image Analysis. Springer, Berlin, Heidelberg https://doi.org/10.1007/3-540-29711-1 (439 pp.).
Rocha-Campos, A.C., dos Santos, P.R., Canuto, J.R., 2008. Late Paleozoic glacial deposits of Brazil: Paraná Basin. In: Fielding, C.R., Frank, T.D., Isbell, J.L. (Eds.), Resolving the Late Paleozoic Ice Age in Time and Space. GSA Special Papers441. https://doi.org/10.1130/2008.2441(07).
Rosa, E.L.M., Isbell, J.L., 2021. Late Paleozoic Glaciation. In: Alderton, D., Elias, S.A. (Eds.), Encyclopedia of Geology, Second edition Academic Press, pp. 534–545 https://doi.org/10.1016/B978-0-08-102908-4.00063-1.
Rosa, E.L.M., Vesely, F.F., França, A.B., 2016. A review on late Paleozoic ice-related erosional landforms in the Paraná Basin: origin and paleogeographical implications. Brazilian Journal of Geology 46, 147–166. https://doi.org/10.1590/2317-4889201620160050.
Sayler, K., 2022. Landsat 8–9 Collection 2 (C2) Level 2 Science Product (L2SP) Guide. https://d9-wret.s3.us-west-2.amazonaws.com/assets/palladium/production/s3fs-public/media/files/LSDS-1619_Landsat-8-9-C2-L2-ScienceProductGuide-v4.pdf. (Accessed 2 January 2023).
Schlüter, T., 2006. Geological Atlas of Africa. Springer, Berlin, Heidelberg (272 pp.).
Senalp, M., Al-Laboun, A., 2000. New evidence on the Late Ordovician Glaciation in Central Saudi Arabia. Saudi Aramco Journal of Technology 11–40.
Stokes, C.R., Clark, C.D., 2001. Palaeo-ice streams. Quaternary Science Reviews 20, 1437–1457. https://doi.org/10.1016/S0277-3791(01)00003-8.
Stokes, C.R., Clark, C.D., 2002. Are long subglacial bedforms indicative of fast ice flow? Boreas 31, 215–302. https://doi.org/10.1111/j.1502-3885.2002.tb01070.x.
Suhet, 2015. Sentinel-2 User Handbook Issue 1 Revision 2. https://sentinels.copernicus.eu/documents/247904/685211/Sentinel-2_User_Handbook.pdf/8869acdf-fd84-43ec-ae8c-3e80a436a16c?t=1438278087000. (Accessed 6 March 2023).
Tofaif, S., Le Heron, D.P., Melvin, J., 2018. Development of a palaeovalley complex on a Late Ordovician glaciated margin in NW Saudi Arabia. Geological Society, London, Special Publications 475, 81–107. https://doi.org/10.1144/SP475.8.
Torsvik, T.H., Cocks, L.R.M., 2011. The Palaeozoic palaeogegraphy of Central Gondwana. Geological Society, London, Special Publications 357, 137–166. https://doi.org/10.1144/SP357.8.
Torsvik, T.H., Cocks, L.R.M., 2013. Gondwana from top to base in space and time. Gondwana Research 24, 999–1030. https://doi.org/10.1016/j.gr.2013.06.012.
Vesely, F.F., Assine, M.L., 2014. Ice-keel scour marks in the geological record. Evidence from Carboniferous soft-sediment striated surfaces in the Paraná Basin, southern Brazil. Journal of Sedimentary Research 84, 26–39. https://doi.org/10.2110/jsr.2014.4.

Vesely, F.F., Assine, M.L., França, A.B., Paim, P.S.G., Rostirolla, S.P., 2021. Tunnel-valley fills in the Paraná Basin and their implications for the extent of late Paleozoic glaciation in SW Gondwana. Journal of South American Earth Sciences 106, 102969. https://doi.org/10.1016/j.jsames.2020.102969.

Vogt, M.-L., Pera, S., Hamit, A., Haeberlin, Y., Bünzli, M.-A., 2013. Hydrochemical exploration of Ennedi, Northern Chad. Swiss Geoscience Meeting 2013, Lausanne, Switzerland pp. 491–492.

Wolff, J.P., 1964. Carte géologique de la République du Tchad. Orléans, France, Bureau de Recherches Géologiques et Minières, scale 1:1,500,000.

Woodworth-Lynas, C.M.T., Dowdeswell, J.A., 1994. Soft-sediment striated surfaces and massive diamicton facies produced by floating ice. In: Deynoux, M., Domack, E., Eyles, N., Fairchild, I., Young, G. (Eds.), Earth's Glacial Record (World and Regional Geology). Cambridge University Press, pp. 241–259 https://doi.org/10.1017/CBO9780511628900.019.

Zaki, A.S., Pain, C.F., Edgett, K.S., Castelltort, S., 2021. Global inventory of fluvial ridges on Earth and lessons applicable to Mars. Earth-Science Reviews 216, 103561. https://doi.org/10.1016/j.earscirev.2021.103561.